Fire Tests on Loaded Steel-Concrete Composite Slabs

Dr. J. Rodríguez, Dr. Luis Lacoma
(Principia, Spain);

Mr. J. Niepceron
(EDF, France);

Dr. R. Cheriguene
(Principia, France).

Abstract

Under project Science, tests were performed on steel-concrete composite slabs to evaluate their performance in fire scenarios. The object of the exercise was to gain knowledge about their behaviour during accidental fires and to improve the existing capabilities for predicting the time evolution of such incidents.

Several different tests were conducted, in which a permanent load is maintained on a slab while the gas temperatures under the slab evolve for 2.5 hours according to the history given in ISO 834. The paper is focused on one of the tested slabs, namely a simply supported slab.

The analyses conducted involve both blind simulations and post test calculations of the fire tests. All the computational work is based on the numerical simulation of the thermal-mechanical problems posed by the applied loads and thermal conditions. The analyses were carried out with Abaqus (SIMULIA, 2014). A damage plasticity model was used to represent the behaviour of mass concrete and standard elastoplastic models were employed for the steel. The temperature dependence was taken into account in all the material properties.

Purely thermal analyses were conducted first for all the problems to establish the temperature distributions at various times, thus providing the material deterioration experienced at each time and location. Using the thermal information, mechanical analyses were carried out to determine the expected time of failure or, if failure was not expected within the 2.5 hours, the remaining safety margin at the end of the test. Finally, post-test calculations were performed refining the initial hypotheses and assumptions.

1. Description of the test

The configuration consists of a horizontal slab simply supported at both ends. Downward loads will be applied on the slab and the fire will take place underneath.

Figure 1 shows a drawing of the slab, including the lower steel plate and the connecting studs.

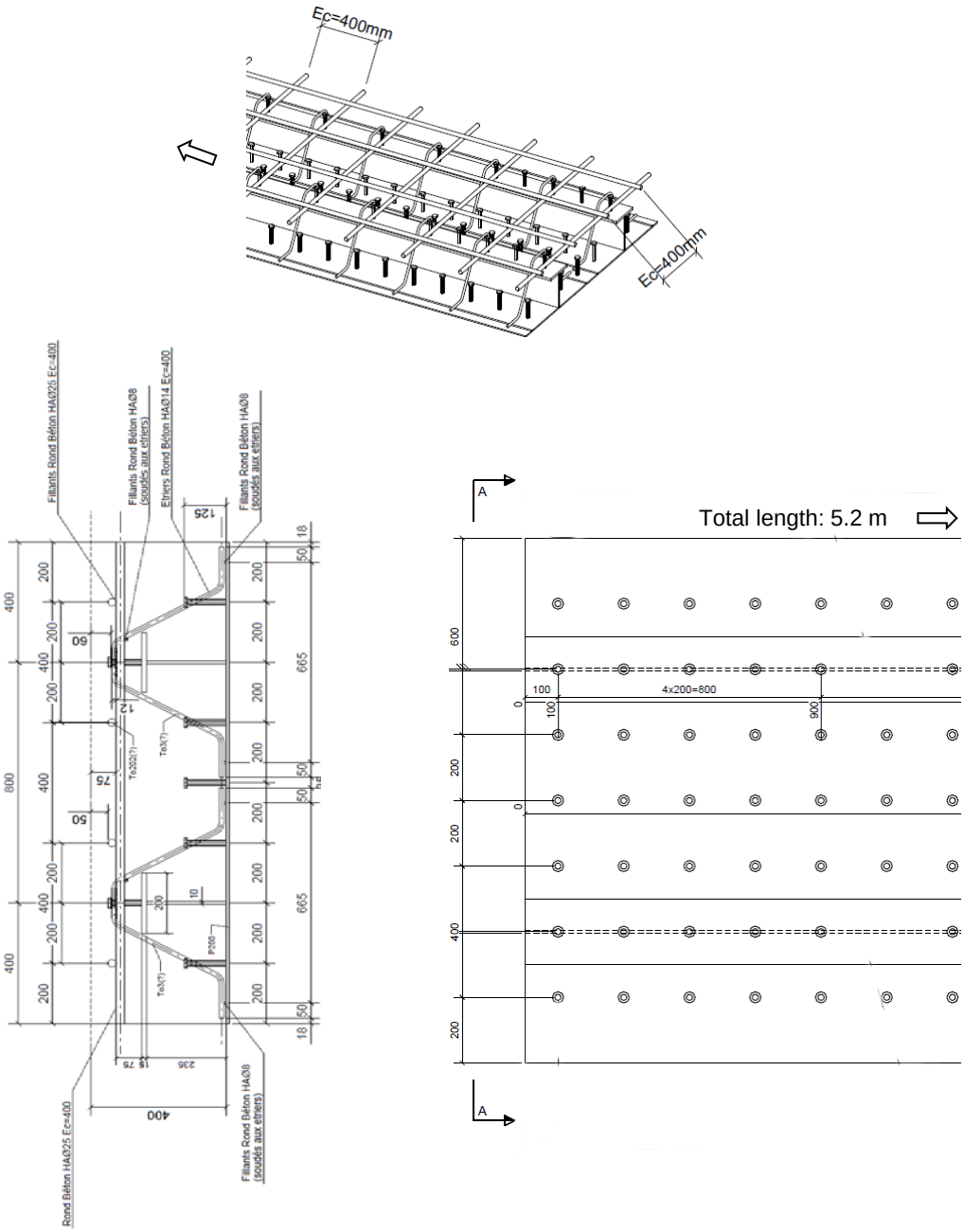

Figure 1: Drawing of the slab

The materials used in the construction of the structure are concrete and steel. The concrete is C30/37 concrete. The steel used for the reinforcing bars in B500S steel. In the case of the steel plate, the material is S355 steel. The steel-concrete connection is achieved with Nelson connecting studs, always with a diameter of 19.05 mm; however, some of the studs are 100 mm long while others are 125 mm.

The thermal conditions imposed by the fire on the exposed surface correspond to those specified by the standard fire curve given in ISO-834 (ISO, 2014).

From a mechanical point of view two types of loads act on the floor specimen: gravity and the applied loads. The gravity loads include the weight of the specimen itself, as well as that of the loading system, which consists of the beams placed at the top of the specimen, with a weight of 22 kN. Apart from the gravity loads, a load is applied during the 150 min of the fire test. The manner of application of the load appears in Figure 2. The value of the load applied, including the weight of the loading system, remains constant during the test at 142.25 kN + 22 kN = 164.25 kN. If failure conditions have not developed yet at the end of the fire test, the previous load starts to be gradually increased at a rate of about 30 kN/min until a failure condition develops.

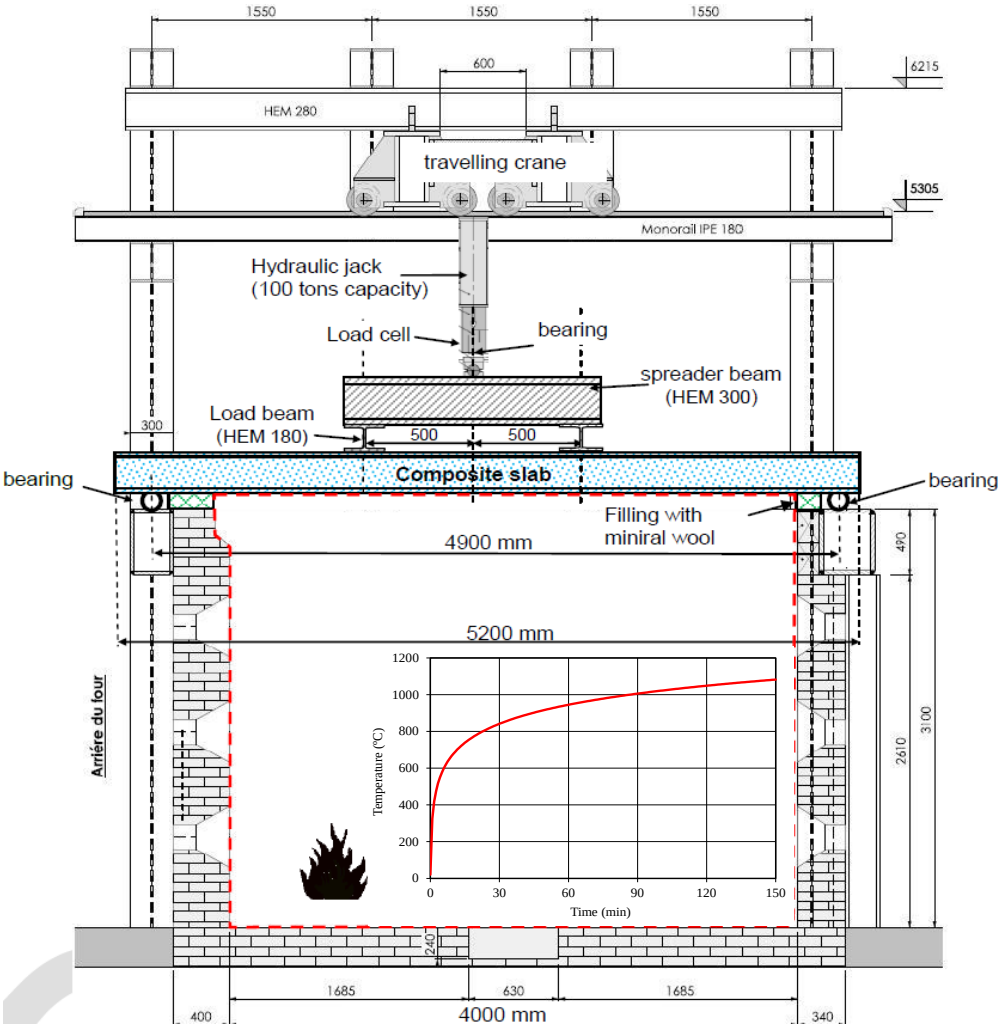

Figure 2: Loads

Two types of failure criteria are used, corresponding to the two functions entrusted to the structure. One is to provide some thermal insulation in order to prevent ignitions from developing on the other side of the slab, which would effectively allow the fire to go across the element. This is implemented by limiting the temperatures developed on the other side of the element across from the fire. The temperature increment produced there will be limited to 140ºC, with the actual temperature developed remaining below 180ºC. Since the initial temperature is 20ºC, the temperature increment condition is stricter, limiting the maximum temperature to 160ºC.

The second function is to retain the integrity required to satisfy its structural duty. From that viewpoint, failure will be assumed to have occurred if the elongation developed by the reinforcing bars exceeds 5%, or if the peak deflection of the slab reaches $1/20^{th}$ of the span.

2. Numerical model

The models generated comprise the concrete, the plate skins, the beams, the reinforcing bars, and the connecting studs.

Embedded studs in the concrete are joined to the steel shell with a planar connector with nonlinear behaviour. Thus, although the studs are embedded in the concrete, they do not share nodes with the steel plates. The relative displacements are properly accounted for through connector elements.

Frictional contact exists between steel shells and the concrete with a friction coefficient of 0.2, which is considered low and thus conservative.

The mesh includes at least 8 elements in the beam thickness and an aspect ratio not larger than 4. The geometrical idealisation can be seen in Figure 3, which shows both the idealised geometry and the finite element mesh, which takes advantage of the longitudinal plane of symmetry to reduce the size of the mesh.

In the thermal model, the areas of the studs and bolts located within a symmetry plane have been reduced to one half. In the mechanical problem the changes in dimension are not helpful since areas and inertias are differently affected. Hence, for the studs and bolts located in symmetry planes, the areas and inertias have not been modified but the mechanical properties (Young's modulus, yield stresses and density) have been scaled appropriately.

Similar techniques are used to model the studs and bolts located within symmetry planes in the thermal and mechanical simulations of the rest of the configurations studied.

The thermal model has about 68,000 first-order hexahedral elements and 660 linear elements, with a total number of about 72,000 nodes and degrees of

freedom. The mechanical mesh has about 13,000 reduced-integration, linear hexahedral elements, 1600 reduced-integration linear quadrilateral shell elements, and 1100 beam elements. The total number of nodes is around 18,000 with approximately 57,000 degrees of freedom.

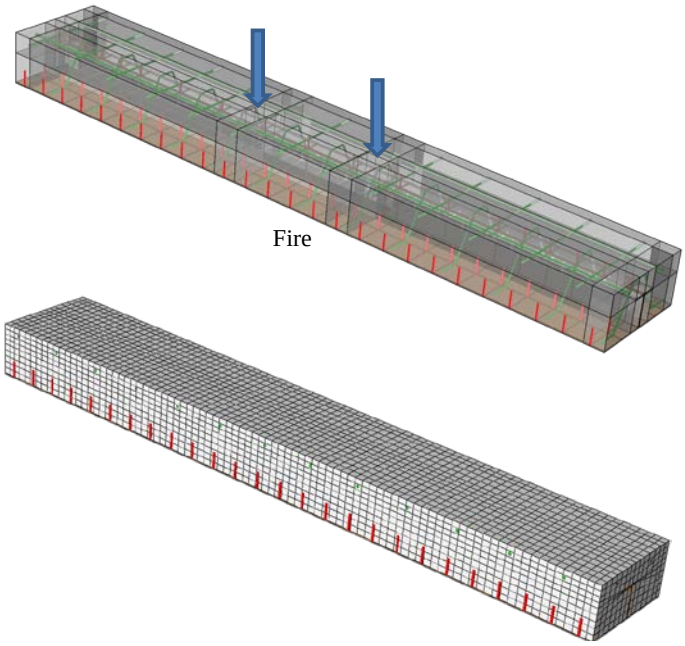

Figure 3: Geometry and finite element mesh

3. Materials

As written in the Eurocodes for fire design, the mechanical properties used in the present calculations are mainly based on steady-state tests. They already incorporate creep effects and the rheological effects are not evaluated separately. As a consequence, the analyses must be expected to produce somewhat greater displacements and lower strengths than the reality that will be manifested in the fire tests.

The thermal and mechanical properties are mainly based on Eurocode 2 Part 1.2 “Structural Fire Design” (CEN, 2008). The properties used are mean properties for the C30/37 designation.

The temperature dependence of the thermal properties of concrete is shown in Figure 4 for the thermal conductivity and Figure 5 for the specific heat. It is worth mentioning that the higher the specific heat, the slower the temperature progression. Besides, the moisture content is not a function only of the w/c ratio. It also depends, for example, on the relative humidity. Figure 5 has been completed showing curves for other values of humidity.

The peak in the specific heat at around 115ºC is caused by the latent heat of water evaporation. Since a high water-cement ratio was used, the highest curve provided by Eurocode 2 was used (corresponding to a moisture content of 3%). The density is assumed 2300 kg/m^3 and decreases according to Eurocode. The rest of the thermal and mechanical properties do not depend directly on the moisture content.

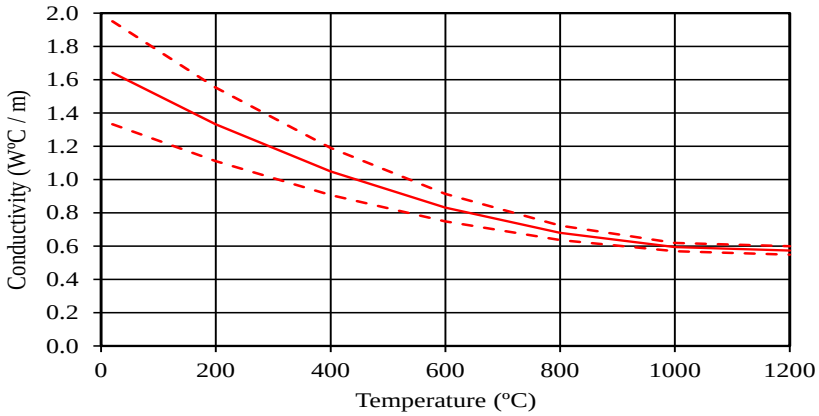

Figure 4: Dependence of the concrete conductivity on temperature

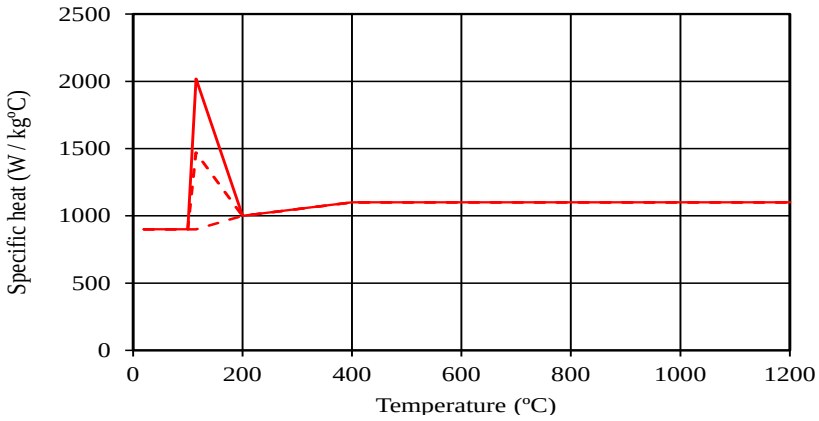

Figure 5: Dependence of the concrete specific heat on temperature

Concerning the mechanical behaviour at normal temperatures, there are some inconsistencies between Part 1 “General Rules and Rules for Buildings” and Part 1.2 “Structural Fire Design” of Eurocode 2. The elastic modulus has been defined here according to Eurocode 2 Part 1, and modified based on the reported strain at peak stress of Eurocode 2 Part 1.2. A bilinear stress-strain curve has been defined at each temperature, reducing the strength and increasing the ultimate strain according to the code.

The concrete damaged plasticity model in Abaqus provides a general capability for the analysis of concrete structures under monotonic, cyclic, and/or dynamic

loading. It includes a scalar (isotropic) damage model with tensile cracking and compressive crushing modes. The model accounts for the stiffness degradation mechanisms associated with the irreversible damage that occurs during the fracturing process.

Since cyclic or reversal effects are not considered important in the simulations, no damage (elastic stiffness degradation caused by the mechanical strain history) is defined in the model.

The effects of varying temperatures on the compressive behaviour of concrete are shown in Figure 6.

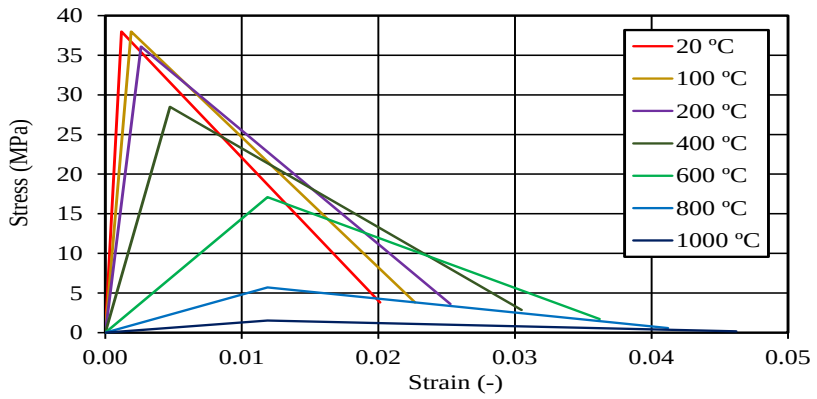

Figure 6: Concrete compressive behaviour at different temperatures

The thermal and mechanical properties adopted for structural steel S355 are mainly based on Eurocode 3 Part 1.2 “Structural Fire Design” (CEN, 2004). The temperature dependence is shown in Figure 7 for the thermal conductivity and Figure 8 for the specific heat. The density is 7850 kg/m^3.

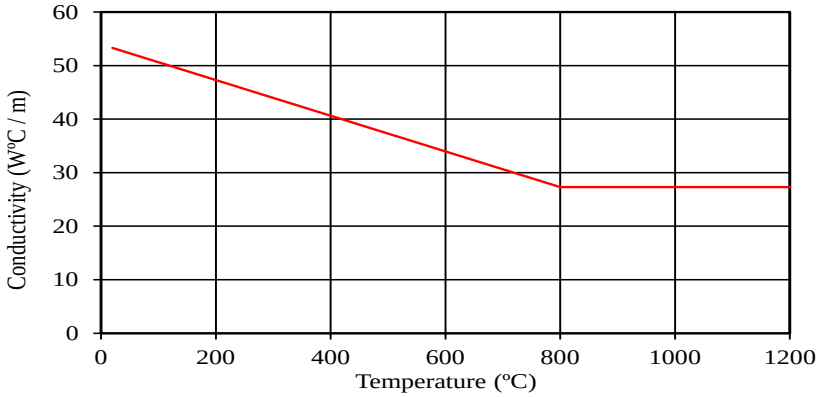

Figure 7: Dependence of the steel conductivity on temperature

Because of the interactions taking place between the two materials, differences in thermal expansion between concrete and steel are particularly relevant.

Figure 9 compares their coefficients of thermal expansion for different temperatures.

From the viewpoint of its mechanical behaviour, the complete stress-strain curves are derived also from Eurocode 3, simplifying to a straight line the behaviour between the proportional limit and the yield strength.

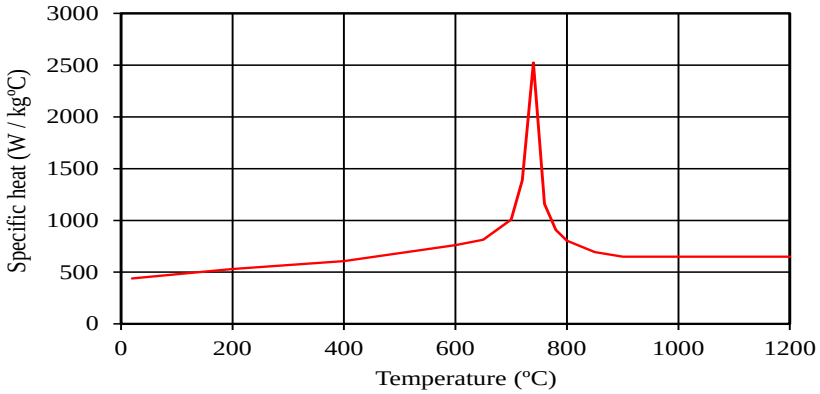

Figure 8: Dependence of the steel specific heat on temperature

Figure 10 shows the curves adopted for different temperatures. Some hardening is assumed, with an ultimate strength (Cauchy) of 600 MPa (within the range for the steel grade), trying to assign more realistic mechanical properties (according to the steel quality the ultimate nominal stress is between 470 and 630 MPa). Besides, the trilinear curves (at proportional limit, 2% and 15%) are expressed as Cauchy stresses and not nominal (engineering) stresses.

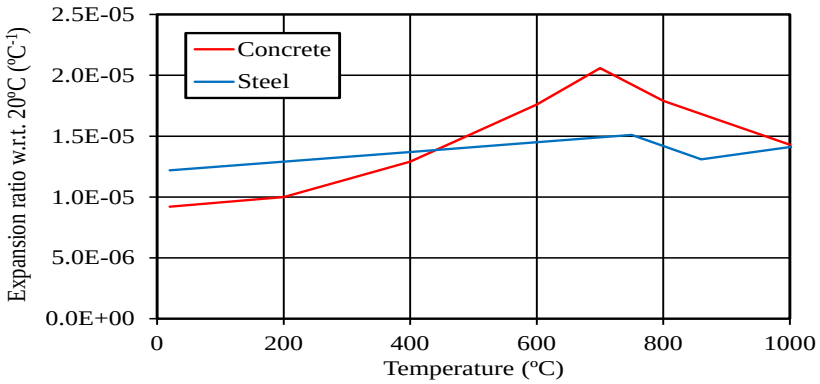

Figure 9: Comparison of the concrete and steel thermal expansion

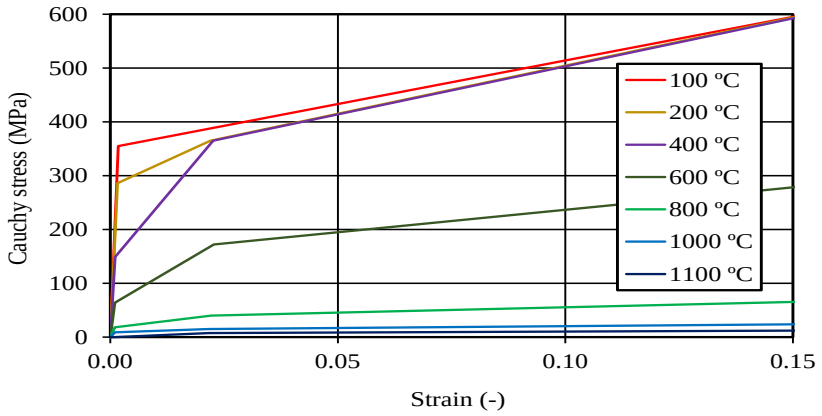

Figure 10: Structural steel behaviour at different temperatures

The shear studs have a diameter of 19.1 mm and 100/125 mm length. The behaviour at normal temperatures of the shear studs is based on Model Code 2010 (FIB, 2010). More specifically, the strength is:

$$P = 5.3 \cdot A \cdot f_c^{0.35} \cdot f_t^{0.65} \cdot (E_c/E_s)^{0.4}, \text{ limited by } A \cdot f_t$$

where $A = \pi(19.1 \text{ mm})^2/4$ is the connector section, f_c = 38 MPa is the compressive strength of concrete, E_c = 32 GPa is the modulus of elasticity of concrete, f_t = 450 MPa is the ultimate tensile stress of steel and E_s = 200 GPa in the modulus of elasticity of steel; resulting P = 129 kN.

This behaviour has been modified for high temperatures according to the reduction coefficients provided by Huang et al. (1999). Similarly to what is done for defining the compressive stiffness of concrete, the stiffness is defined here as the secant slope for a force equal to 40% of the strength, which according to Model Code 2010 corresponds to a relative displacement between the concrete and the steel plate of 0.4 mm. More specifically, the relation between the relative displacement s (mm) and the force is proportional to $[1-\exp(-\beta s)]^{\alpha}$ with representative values of α and β of 0.8 and 1.0, respectively.

The temperature dependence of the stiffness and strength of the studs is shown in Figure 11.

The thermal and mechanical properties adopted for the reinforcing bars are primarily based on Eurocode 2 Part 1.2 “Structural Fire Design” (CEN, 2008). As already indicated they are made of B500S steel.

The factors used to reduce the Young´s modulus and to define the stress-strain relation are obtained from Table 3-2a of the Eurocode 2 Part 1.2. With these parameters the complete stress-strain curves can be defined and they are presented in Figure 12 at different temperatures. More specifically, the hot rolled curves are used to scale the Young’s modulus and the linear plastic

curves. Trying to assign realistic properties, hardening is considered with an ultimate nominal stress of 675 MPa (within the range for the steel grade).

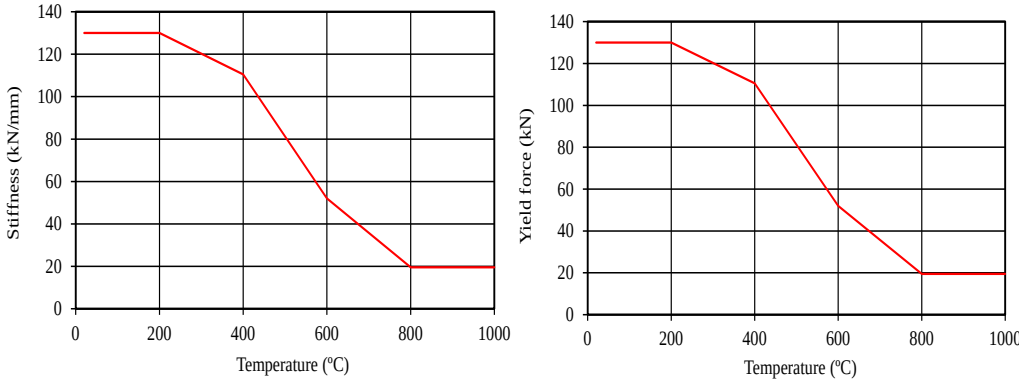

Figure 11: Dependence of the shear stud stiffness (a) and strength (b) on temperature

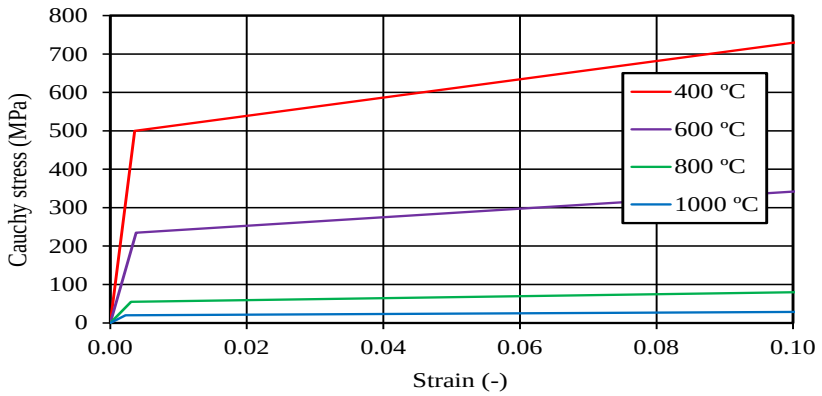

Figure 12: Rebars behaviour at different temperatures

4. Analysis procedure

The thermal and mechanical problems are only weakly coupled since, although the temperatures have a strong influence on the mechanical problem, the mechanical variables have negligible effects on the thermal problem. This allows dealing with the coupling in a sequential manner: the thermal analyses are conducted first and then their results are fed to the mechanical analyses.

The evolving thermal problem is analysed by implicit integration using Abaqus/Standard. The resulting temperatures are interpolated and supplied to the mechanical analyses as required. As already clarified, when conducting the thermal analyses, a heat transfer coefficient of 10 W/m^{2}ºC for the unexposed slab surface governs the heat exchanges with a 20ºC atmosphere. The values of heat transfer coefficients (HTC) are difficult to determine accurately. A value of 10 W/m^{2}ºC for the unexposed surfaces is within the typical range as can be seen in Figure 1.12 of Bejan (1993). The temperature is conservatively

prescribed in the exposed surface as equal to the gas temperature, given the uncertainties in the HTC determination.

The mechanical problem is highly nonlinear. The material behaviour generates the more important nonlinearities, but the geometric nonlinearities are also activated, enabling the modelling of global and local buckling. Frictional contacts are also a source of nonlinearities. This makes the problem awkward for implicit methods and an explicit integration was preferred. To expedite the computations, a mass scaling technique has been used.

The overall analyses involved several successive steps. In a first step the gravity and mechanical loads are introduced smoothly. The thermal load is then applied in a second step lasting 150 min. Finally, the mechanical loads are increased gradually until a failure condition develops.

5. Blind simulations

A thermal analysis is conducted first in order to determine the temperature distributions at different times from the initiation of the fire. Figure 13 shows the temperature distributions developed in the model at 6 different times up to 150 min.

Of special significance is the temperature distribution at the end of 2 hours, since it establishes whether or not, according to ISO 834, the fire insulation function of the slab has been maintained during the test. Neither the peak temperature nor the peak temperature increase exceed the imposed limits. However, the fire test duration was extended for another half an hour, confirming that even at that time the temperatures and temperature increases in the unexposed face satisfy the thermal insulation conditions.

Along the 150 min duration of the fire test, the load is maintained but the temperatures gradually increase; as a consequence, stresses, strains and displacements evolve. Figure 14 indicates the evolution of the peak displacements at mid-span. One of the failure criteria is triggered when the peak displacements attain $1/20^{th}$ of the span, which is 250 mm. If at the end of the 150 min test those displacements have not taken place and no reinforcing bars have yielded above 5%, the applied load is increased at a rate of 30 kN/min until one of those conditions develops. As shown, the expected displacements remain well below the limit after 150 min; the increase experienced after that time is primarily the result of the increments in the applied load.

At the end of the planned duration of 150 min, Figure 15 shows the longitudinal stresses in the concrete, Figure 16 depicts them in the structural steel, Figure 17 describes the equivalent cracking strains, and Figure 18 indicates the plastic strains developed in the structural steel and reinforcing

bars. No failure conditions have been reached at that time and hence the applied load starts to be increased until one of those conditions is attained.

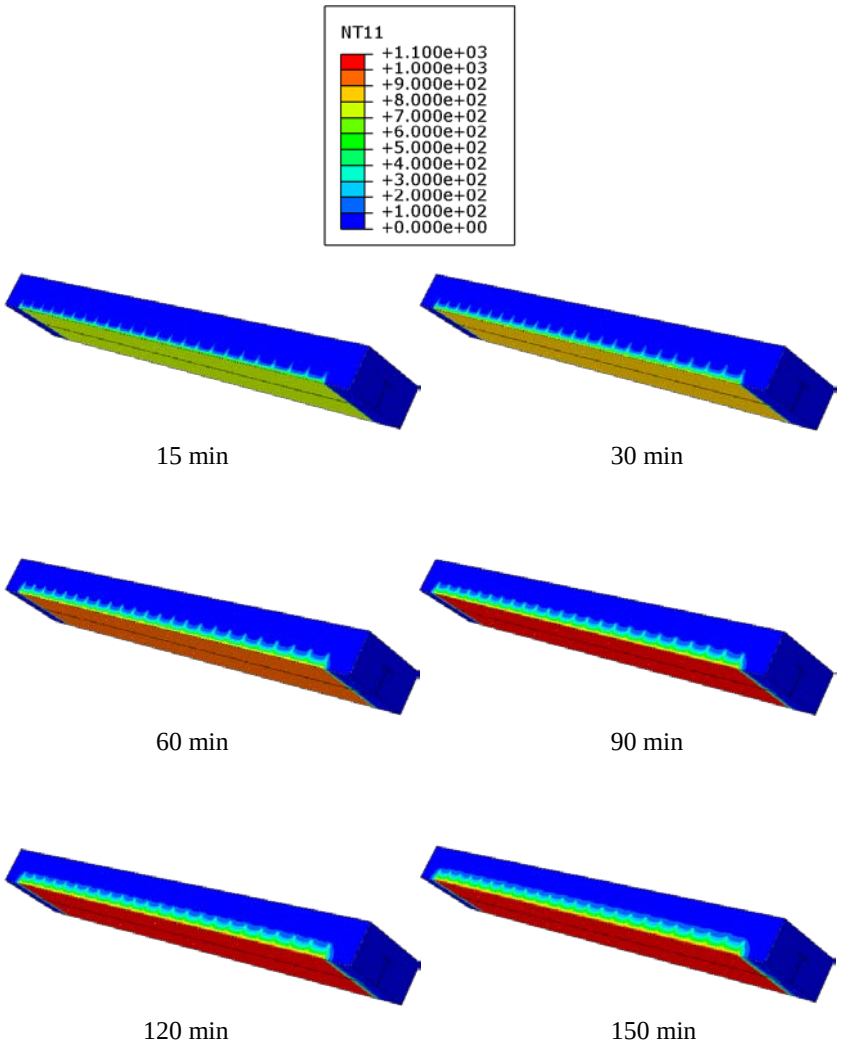

Figure 13: Temperatures at 15, 30, 60, 90, 120 and 150 min

After 150 min the applied load is increased at a rate of 30 kN/min until failure results. The impending failure is triggered by a hinge developed at mid-span. Under the situation at failure the lower steel plate no longer contributes to the mechanical performance. The resulting moments are being handled by tension in the upper steel flange and compression of the concrete at the top. The concrete in the lower part of the cross-section is cracked, as the lower steel plate is no longer able to carry the corresponding tensile stresses.

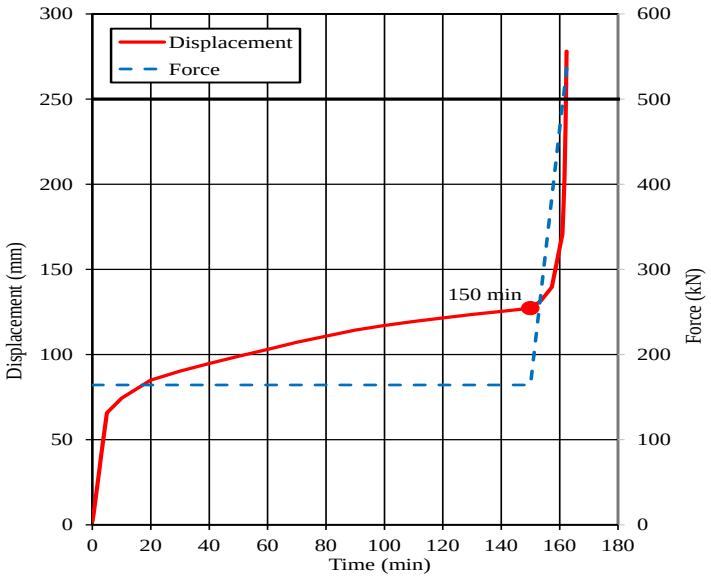

Figure 14: History of displacement at the middle of the span

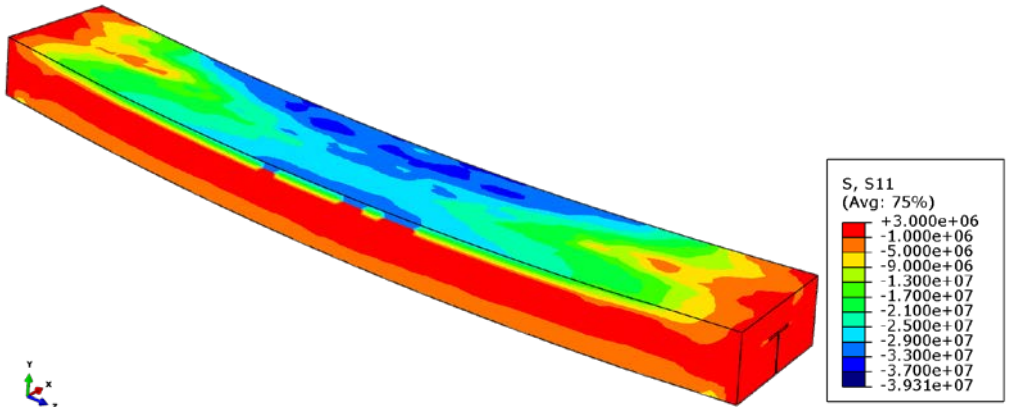

Figure 15: Longitudinal stresses in the concrete at 150 min

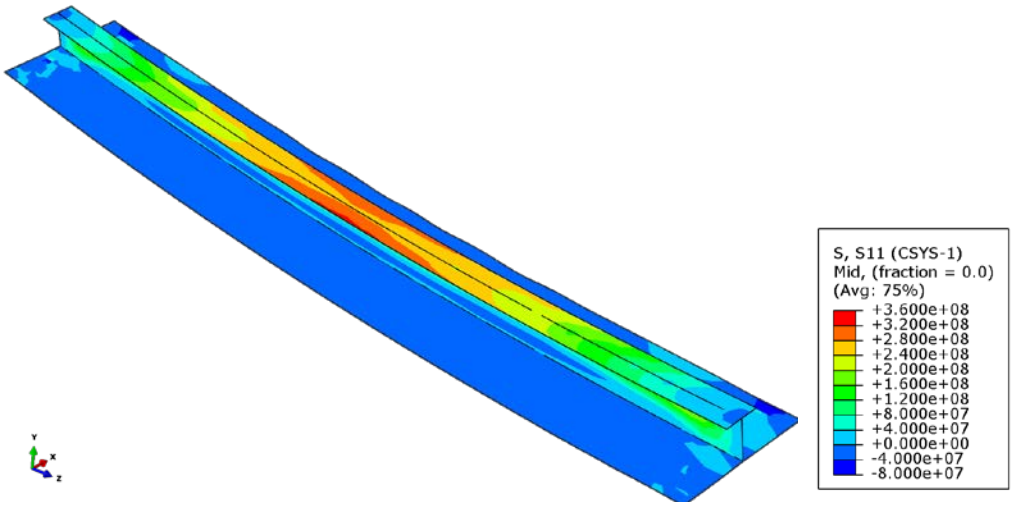

Figure 16: Long. stresses in the structural steel at 150 min

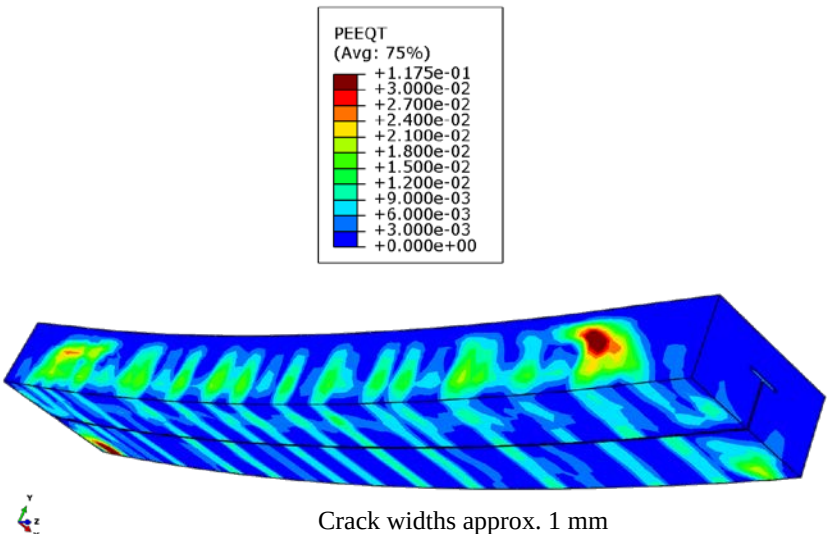

Figure 17: Equivalent cracking strains at 150 min

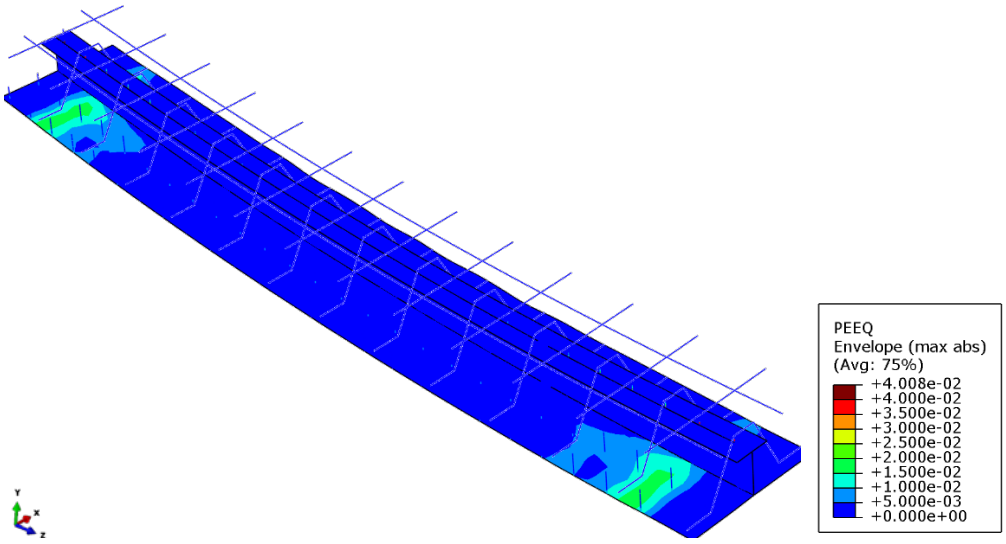

Figure 18: Plastic strains in steel and rebars at 150 min

6. Post-test calculations

6.1 Test data

The test was densely instrumented and especial attention was paid to the data provided by specific sensors capturing temperatures, vertical displacements, and rotations of the slab ends. Because of the nature of experimental data, sensors placed in theoretically identical conditions can be expected to record somewhat different data. Hence, in order to allow comparisons with the calculations, some specific sensors were selected as representative of the conditions experienced.

The load applied to the slab was maintained constant at 142.25 kN for a duration of 150 min. Thereafter, the applied load was linearly increased to reach 618 kN after 163 min, whereupon the test was terminated.

6.2 Temperature distribution

When trying to evaluate whether the numerical results reproduce well the experimental findings, the first concern must be whether the input conditions of the test are being properly represented. The initial calculations assumed that the steel shell next to the fire was actually at the gas temperature mandated by the specification. The measurements, however, showed that this was not the case in reality. During the test, the shell temperatures were seen to lag considerably behind the gas temperatures.

As a consequence, trial and error calculations were conducted to determine a realistic value for the heat transfer coefficient across the steel-gas interface. Those calculations indicated that 100 $W/m^2\,^oC$ is a representative value for the heat transfer coefficient across that interface in the present test.

The thermal calculations were then redone. The comparison between calculated and measured temperatures appears in Figure 19 for the steel profiles and Figure 20 for different locations within the concrete. It can be seen that the comparisons are very reasonable and therefore the hypotheses adopted were considered to be suitable for reproducing the actual conditions.

6.3 Mechanical evolution

The calculated and measured vertical displacements at mid-span and at 1000 mm from mid-span are compared in Figure 21. The calculations predict displacements that are very close to the observed values.

Additionally, an analysis was carried out without considering the thermal expansion of concrete. The displacement history is compared with the measurements in Figure 22. The results are essentially as good as the former ones, slightly lower than the test values. As a consequence, the deformation of the structure seems to be mainly controlled by the thermal expansion of the steel.

6.4 Sensitivity to the stiffness of the studs

The relative displacements between the steel plates and the concrete around the stud are below 1 mm, which is the representative limit for the linear behaviour of the studs.

An additional sensitivity analysis was carried out reducing the stud stiffness by a factor of 2. The resulting history of the displacements is compared in Figure 23 with the baseline simulation. The curves are very similar, as the stiffness of

the studs is not controlling the global behaviour of the structure. Hence a linear behaviour may be adopted without loss of accuracy.

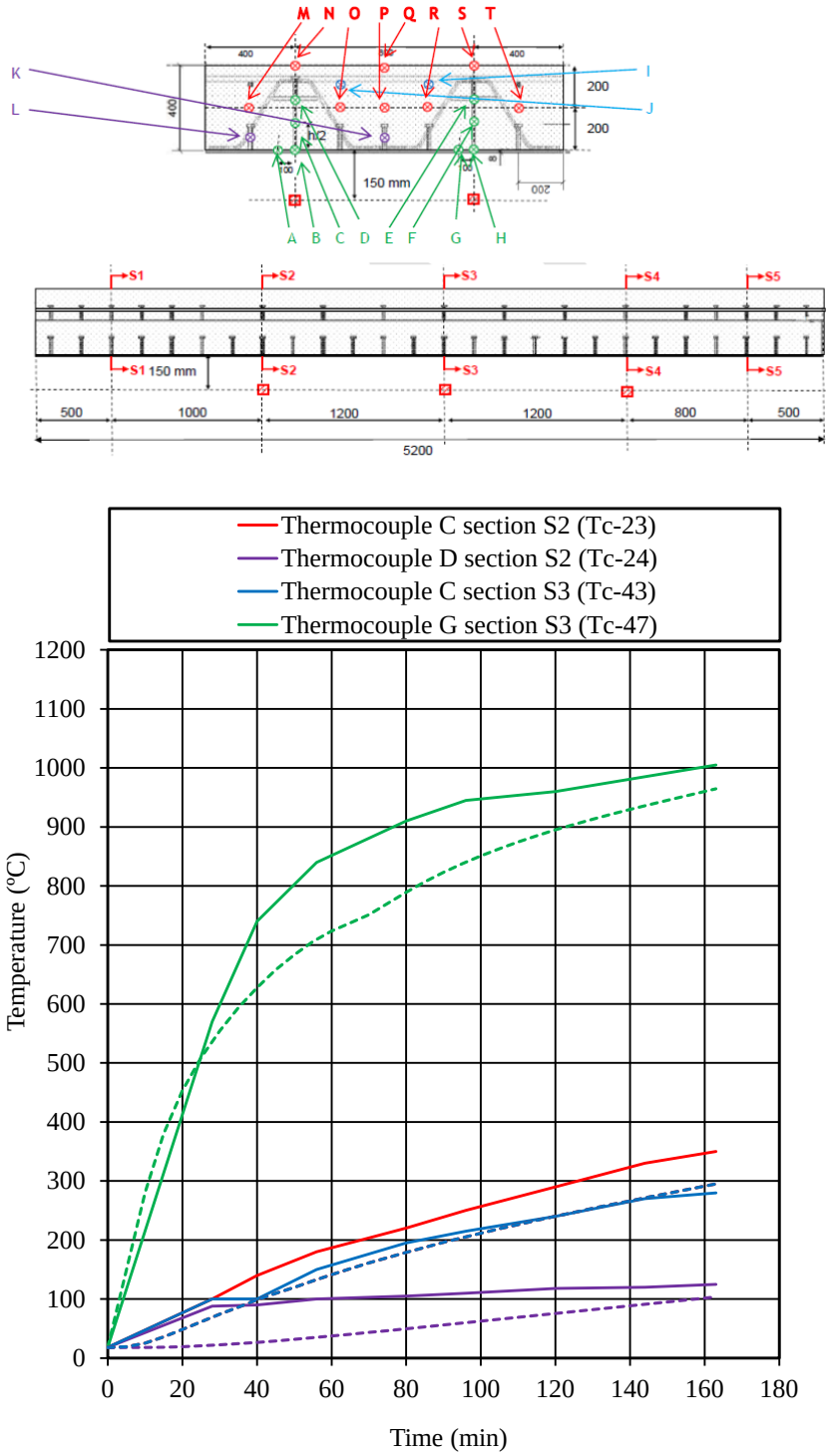

Figure 19: Comparison of temperatures in the steel plates

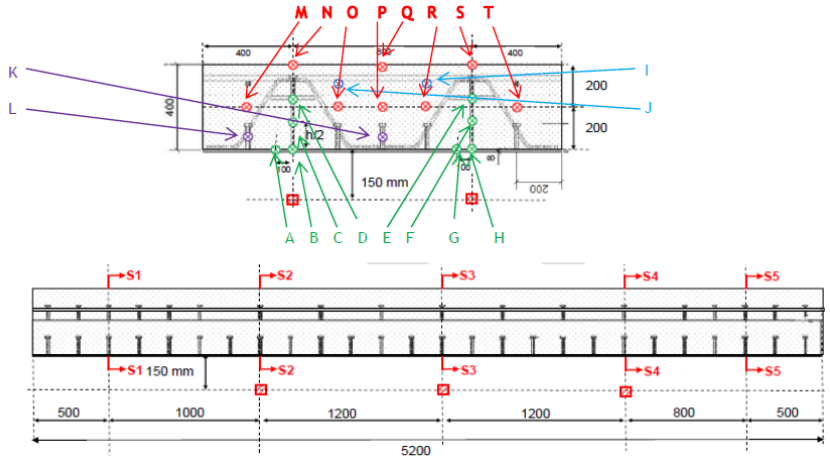

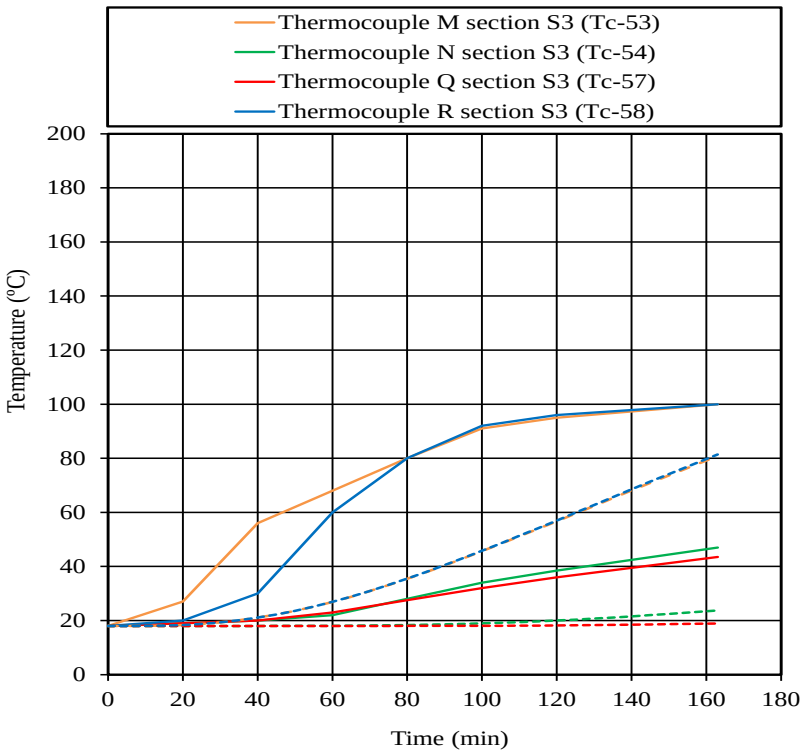

Figure 20: Comparison of temperatures in the concrete

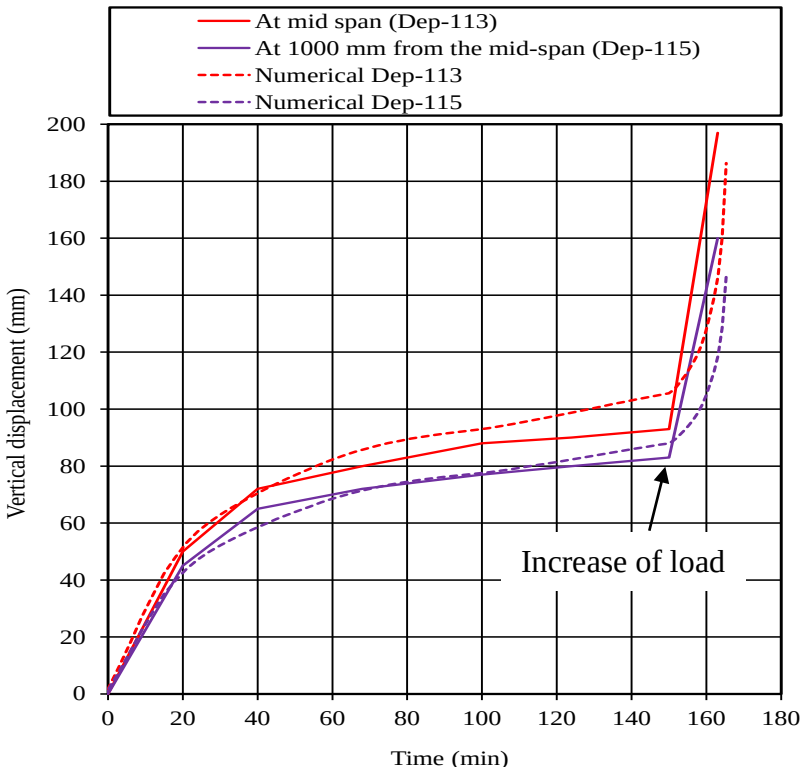

Figure 21: Comparison of vertical displacements

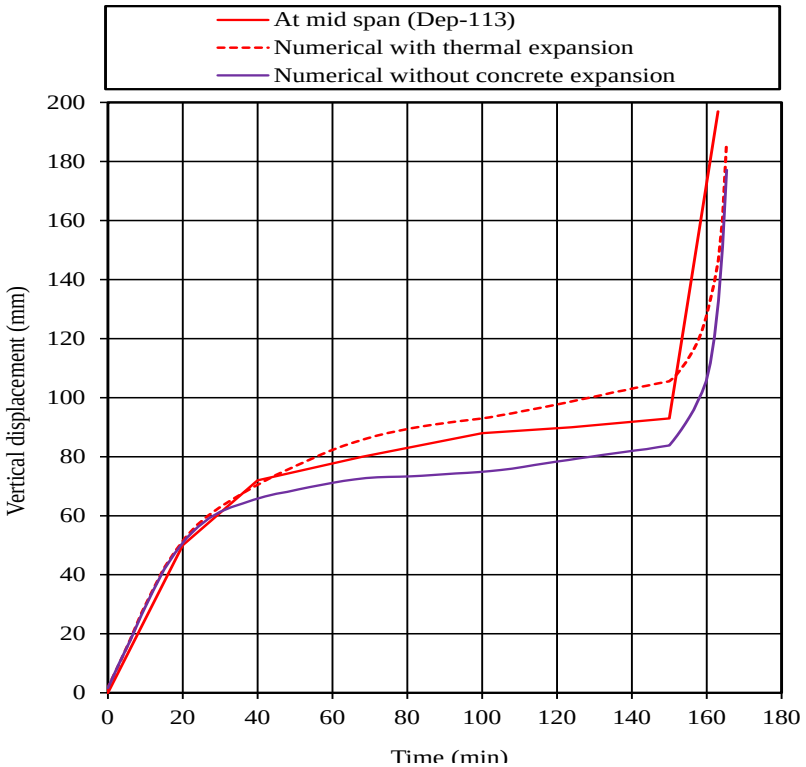

Figure 22: Comparison with and without concrete expansion

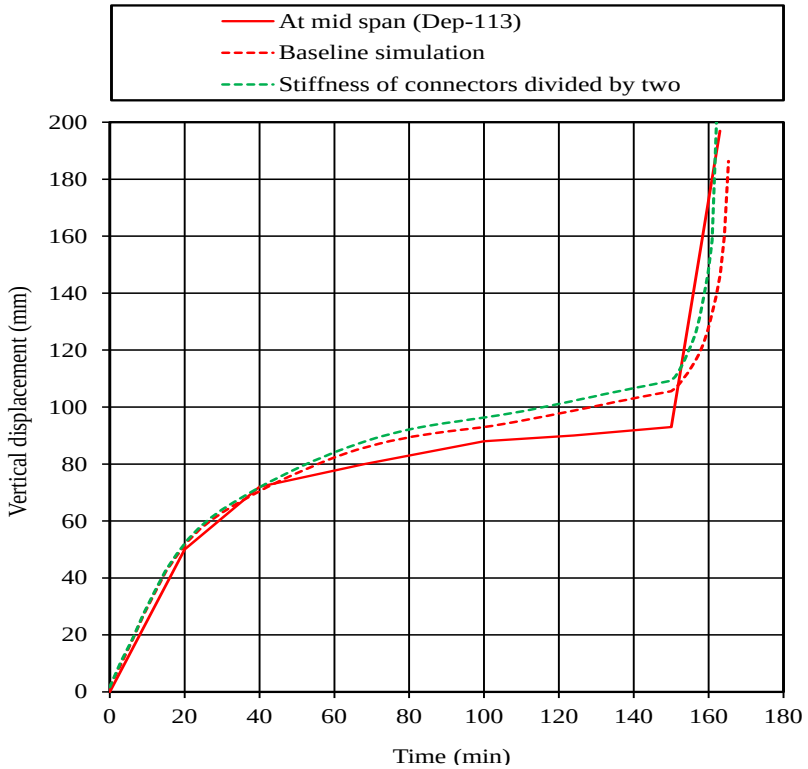

Figure 23: History of disp. with reduced stud stiffness

7. Conclusions

Blind simulations were first conducted to predict the performance of composite steel-concrete slabs that were later subjected to applied forces and imposed fires. Following the tests new calculations were carried out in order to gain further knowledge from the exercise. The configuration studied here is that of a simply supported floor.

The thermal variables have a strong influence on the mechanical behaviour, but there is practically no influence of the mechanical variables on the thermal problem. This allows dealing with the problem sequentially, i.e.: a thermal followed by a mechanical analysis. The thermal problem is only moderately nonlinear and can be solved implicitly; by contrast, the mechanical models include highly nonlinear effects and an explicit solver was used.

From the work performed, some conclusions can be offered:

a) The pre-test simulations were conservative, in the sense that the temperatures calculated in the unexposed surface and the calculated displacements were somewhat higher than observed in the test.

b) A heat transfer coefficient on the order of 100-200 W/m^2 ºC is adequate for modelling the heat exchange across the exposed surface of the structure.

This coefficient represents a complex combination of radiation, convection and conduction processes.

c) Most of the deformations taking place are controlled by the thermal expansion of the steel plates. Indeed, the calculations match better the measurements if the concrete expansion is neglected. Standard calculations tend to overestimate the effective thermal expansion of cracked concrete, which is likely to be rather small.

d) The strength of the shear studs is sufficient for transmitting the shear forces and the relative displacements between the concrete and steel plates have a negligible effect on the deformation of the structure. Some local buckling has been detected but has no effect on the global response.

e) In the material properties provided for the steel, creep effects are not considered separately. But such effects explain the displacement reversals observed, leading to an overprediction of the displacements. The results improve if the thermal expansion coefficient of steel is kept at its 20ºC value, neglecting its increase with temperature.

8. References

Bejan, A. (1993) "*Heat Transfer*", John Wiley and Sons, Inc.

CEN – European Committee of Standardization (2008) "*EN 1992. Eurocode 2: Design of Concrete Structures*".

CEN – European Committee of Standardization (2004) "*EN 1993. Eurocode 3: Design of Steel Structures*".

CTICM (2015) "*SC for Industrial, Energy and Nuclear Construction Efficiency (SCIENCE). Report on Fire Tests*", report no. RFSR-CT-2014-00017 version B, 18 November.

FIB – International Federation for Structural Concrete (2010) "*fib Model Code for Concrete Structures 2010*".

Huang, Z., Burgess, I.W., and Plank, R.J. (1999) "The Influence of Shear Connectors on the Behaviour of Composite Steel-Framed Building in Fire", *Journal of Constructional Steel Research*, Vol. 51, pp. 219-237.

ISO – International Standards Organization (2014) "*ISO 834. Fire Resistance Tests*".

SIMULIA (2014) "*Abaqus Analysis User's Manual*", Version 6.14, Providence, Rhode Island.